

Jamming in Systems Composed of Frictionless Ellipse-Shaped Particles

Mitch Mailman,¹ Carl F. Schreck,² Corey S. O'Hern,^{3,2} and Bulbul Chakraborty¹

¹*Martin Fisher School of Physics, Brandeis University, Mail Stop 057, Waltham, Massachusetts 02454-9110, USA*

²*Department of Physics, Yale University, New Haven Connecticut 06520-8120, USA*

³*Department of Mechanical Engineering, Yale University, New Haven, Connecticut 06520-8284, USA*

(Received 5 December 2008; revised manuscript received 24 April 2009; published 22 June 2009)

We study numerically frictionless ellipse packings versus the aspect ratio α , and find that the jamming transition is fundamentally different from that for spherical particles. The normal mode spectra possess two gaps and three distinct branches over a range of α . The energy from deformations along modes in the lowest-energy branch increases quartically, not quadratically. The quartic modes cause novel power-law scaling of the static shear modulus and their number matches the deviation from isostaticity. These results point to a new critical point at $\alpha > 1$ that controls jamming of aspherical particles.

DOI: 10.1103/PhysRevLett.102.255501

PACS numbers: 61.43.-j, 63.50.Lm, 81.05.Kf, 83.80.Fg

A decade ago, Liu and Nagel proposed [1] that the onset of jamming in disordered systems such as granular materials, colloids, and foams, where thermal fluctuations are unimportant, is controlled by a special second-order critical point (Point J) [2]. A key ingredient in theoretical descriptions of jammed systems is that they must satisfy force and torque balance. In a static granular packing, mechanical stability can be achieved only if the number of contacts satisfies $N_c \geq N_d$, where N_d is the number of degrees of freedom [3]. For N frictionless spherical grains in d dimensions, static packings at Point J are *isostatic* [4,5] with $N_c = Nd$. Important properties of systems near Point J , such as power-law scaling of the structural and mechanical properties [2] and soft modes in the vibrational spectra [6] have been attributed to isostaticity of packings of frictionless, spherical grains.

In contrast to static packings of frictionless, spherical particles, ellipsoid packings are hypostatic [7,8] with $N_c < N_d$. The stability of hypostatic packings can be understood in terms of “quartic” modes in their vibrational spectra [7,8]. The quartic modes impart stability by preventing only finite-amplitude motions, in contrast to quadratic modes that cost energy even for infinitesimal displacements. The hypostatic nature of ellipsoid packings raises fundamental questions, for example, how does hypostaticity alter low-energy excitations and mechanical response?

We investigate jamming of frictionless ellipses using simulations of soft particles with purely repulsive interactions at zero temperature. Static 2D packings are an important paradigm for understanding jamming in granular systems since gravity does not play a role, accurate measurements of grain contacts and forces can be obtained [9], and grain-level tests of theoretical predictions can be performed [10]. We find significant differences between the behavior near jamming of ellipse-shaped and spherical particles: (i) The lowest-energy vibrational excitations are composed of predominantly rotational particle motion. The mean-square frequency of these modes scales with packing fraction ϕ and aspect ratio α as $\langle \omega_1^2 \rangle \propto$

$(\phi - \phi_J)(\alpha - 1)$, where ϕ_J is the jamming packing fraction. At ϕ_J , the energy from deformations along these “quartic” modes increases quartically, not quadratically. (ii) The number of quartic vibrational modes near jamming exactly matches the deviation in the contact number from the isostatic value. (iii) The number and energy of the quartic modes determines the power-law scaling of the static shear modulus $G = G_0(\phi - \phi_J)^\tau$, where $\tau = 1$, which is different from that for spherical particles ($\tau = 0.5$). These results suggest that the mechanical properties of ellipses are not controlled by purely translational soft modes characteristic of point J .

Compression packing-generation protocol.—We generated static packings of frictionless ellipses at ϕ_J in systems with $N = 120$ to 1920 particles, using a numerical protocol similar to that employed to create packings of spherical particles [11,12]. In this method, soft, purely repulsive ellipses are initially randomly placed in a square cell with periodic boundaries at $\phi = 0.5$. The configurations are successively compressed in small steps ($\delta\phi = 10^{-4}$) and then relaxed using energy minimization after each step. Near ϕ_J , the configurations are expanded or compressed by decreasing amounts until the system has vanishingly small total potential energy per particle $V_{\min} < V < 2V_{\min}$. We set $V_{\min} = 10^{-16}$, which implies that we can locate ϕ_J to within 10^{-8} . We employed the linear repulsive spring potential with the Perram and Wertheim overlap parameter σ_{ij} [13–16].

The vector \hat{r}_{ij} between centers of mass and orientations \hat{u}_i and \hat{u}_j of particles i and j determine

$$\sigma_{ij} = \min_{\lambda} \frac{\sigma_0(\lambda)}{\sqrt{1 - \frac{\chi(\lambda)}{2} \sum_{\pm} \frac{\beta(\lambda) \hat{r}_{ij} \cdot \hat{u}_i \pm \beta^{-1}(\lambda) \hat{r}_{ij} \cdot \hat{u}_j}{1 \pm \chi(\lambda) \hat{u}_i \cdot \hat{u}_j}}}, \quad (1)$$

where σ_0 , β , and χ depend on λ and the major (minor) axes, a (b), of the particles [13]. Minimization of (1) with respect to $0 < \lambda < 1$ must be performed to determine σ_{ij} for each pair of particles. We simulate bidisperse mixtures in which one-third of the particles are large with the major

axis 1.4 times that of the small particles [7] to suppress ordering. We generated at least 100 packings, each characterized by ϕ_J , from $\alpha = a/b = 1$ to 2.

Vibrational spectra.—The mechanical stability of static packings can be probed using the dynamical matrix $M_{mn} = \partial^2 V / \partial \vec{\xi}_m \partial \vec{\xi}_n$, whose eigenmodes describe low-energy excitations [17]. For ellipses, $\vec{\xi}_m = \{x_m, y_m, a_m \theta_m\}$, where x_m and y_m are center of mass coordinates for particle m , θ_m characterizes the particle's orientation, and $m, n = 1, \dots, N$. With periodic boundaries, M_{mn} has $(2d - 1)\mathcal{N} - d$ nontrivial eigenvalues, where $\mathcal{N} = N - N_r$ and N_r is the number of “rattler” particles that are not locally stable. If all particles have the same mass, the square roots of the eigenvalues of M_{mn} (normalized by \mathcal{N}) give the normal mode frequencies ω_i indexed by i , with eigenvectors $\hat{e}_i = \{e_{xi}^{j=1}, e_{yi}^{j=1}, e_{\theta i}^{j=1}, \dots, e_{xi}^{j=\mathcal{N}}, e_{yi}^{j=\mathcal{N}}, e_{\theta i}^{j=\mathcal{N}}\}$ that satisfy $\hat{e}_i^2 = 1$.

Over a range of α , the spectrum ω_i , sorted in order of increasing frequency, possesses three distinct regimes (cf. Fig. 1): (1) modes with indices $i < i^*(\alpha)$ below the low-frequency gap, (2) modes with $i^* \leq i \leq i_t = (d - 1)\mathcal{N}$, where for $\alpha \leq \alpha_t$, there is a second gap at index i_t , and (3) modes with $i > i_t$. (We do not include the d modes corresponding to translational invariance.) In the inset to Fig. 1, we show that we are able to choose aspect ratio dependent scaling factors ω^* and i^* that collapse the low-frequency part of the spectra including the first gap. We find that ω^* scales as $\sim(\alpha - 1)$, while i^* possesses different scaling regimes for $\alpha - 1 \ll 1$ and $\alpha \geq 1$. Below, we use the scaling of i^* to relate the vibrational spectra to hypostaticity of ellipse packings. We use the eigenvectors to calculate the contributions of translations, $T_i = \sum_{j=1}^{\mathcal{N}} \{(e_{xi}^j)^2 + (e_{yi}^j)^2\}$, and rotations, $R_i = 1 - T_i$ to mode i . As demonstrated in the inset to Fig. 2, modes in regions 1 and 2 (3) are mainly rotational (translational).

Hypostaticity and quartic modes.—As in previous studies [7], we find that ellipse packings are hypostatic (cf. Fig. 3). Analysis of the vibrational spectra shows that ellipse packings at finite overcompression possess $(2d - 1)\mathcal{N} - d$ nonzero, positive eigenvalues of the dynamical matrix. If this behavior were to persist to zero overcompression, it would imply that these systems are isostatic, not hypostatic. To resolve this puzzle, we investigated the vibrational modes versus overcompression.

We perturbed ellipse packings along each of the eigen-directions of the dynamical matrix over a range of overcompression $\Delta\phi \equiv \phi - \phi_J$. If $\vec{\xi}_0$ characterizes the centers of mass and orientations of the original packing, the perturbed configuration obtained after a shift by δ along eigenmode i and relaxation to the nearest local energy minimum is $\vec{\xi}_i = \vec{\xi}_0 + \delta \hat{e}_i$. In Fig. 2, we plot the change in potential energy, $\Delta V_i \equiv V(\vec{\xi}_i) - V(\vec{\xi}_0)$, from a perturbation along mode i versus the amplitude δ for $N = 120$, $\alpha = 1.5$, and two values of $\Delta\phi$. As shown in Fig. 2, for modes with indexes in regions (2) and (3) of the

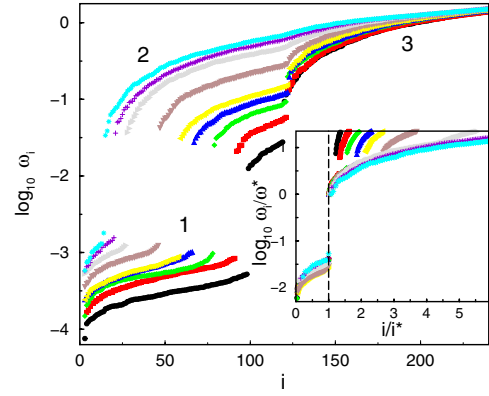


FIG. 1 (color online). Normal mode frequencies ω_i from the dynamical matrix vs index i , sorted by increasing frequency for $N = 120$ ellipse packings at nine aspect ratios, $\alpha = 1.02$ (black), 1.04 (red), 1.06 (green), 1.08 (blue), 1.1 (yellow), 1.2 (brown), 1.4 (gray), 1.6 (violet), and 1.8 (turquoise). There are three distinct branches numbered 1, 2, and 3. In the inset, we show the scaled frequency ω_i/ω^* vs i/i^* , which collapses the low-frequency spectra at $i/i^* = 1$ (vertical dashed line).

frequency spectrum, $\Delta V_i \propto \delta^2$ for all δ independent of $\Delta\phi$. In contrast, there is range $\delta > \delta_c$ over which modes in region (1) display *quartic* dependence on δ , $\Delta V_i \propto \delta^4$, whereas $\Delta V_i \propto \delta^2$ for $\delta < \delta_c$. We find that $\delta_c \sim \Delta\phi^{1/2}$ for modes in region 1, and therefore quartic behavior persists over the entire range of δ in the zero-compression limit. Thus, “just-touching” ellipse packings are stabilized by quartic terms in the expansion of the potential energy around the reference packing [7]. Moreover, even though quartic modes attain a small amplitude quadratic contribution at nonzero $\Delta\phi$, the quartic branch remains distinct

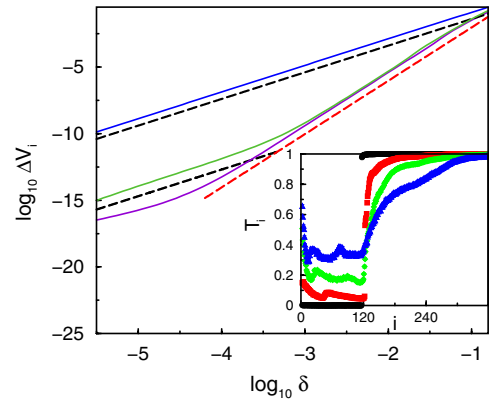


FIG. 2 (color online). Change in potential energy ΔV_i vs displacement δ along \hat{e}_i for $N = 120$ and $\alpha = 1.5$ ($i^* = 22$). ΔV_i (solid blue) for $i = 115 > i^*$ is quadratic in δ . In contrast, for $i \leq i^*$, $\Delta V_i \propto \delta^2$ for $\delta < \delta_c$, but $\Delta V_i \propto \delta^4$ for $\delta > \delta_c$. For $i = 24$, we show that δ_c decreases from approximately 10^{-3} to 10^{-4} as $\Delta\phi$ varies from 10^{-6} (green) to 10^{-8} (purple). The dashed black (red) line has slope two (four). Inset: The translational contribution T_i to the sum of the squares of the amplitudes of each eigenvector \hat{e}_i of the dynamical matrix for $\alpha = 1.01$ (black), 1.2 (red), 1.5 (green), and 2.0 (blue).

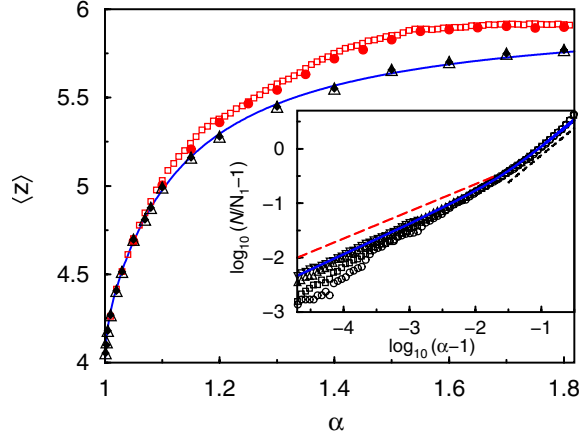


FIG. 3 (color online). Contact number $\langle z \rangle$ vs α for compression (triangles) and shape-annealing [$\Delta\alpha = 0.005$ (open squares) and 0.05 (closed circles)] packing-generation methods for $N = 480$. The filled diamonds represent $\langle z \rangle$ from Eq. (2) for compression. The inset shows system size dependence of $\mathcal{N}/N_1 - 1$ for compression, where N_1 is the number of quartic modes, for $N = 120$ to 1920 (from bottom to top). The red (black) dashed line has slope 0.5 (1.0). The solid line interpolates between power laws of 0.5 (1.0) for $\alpha - 1 \ll 1$ ($\alpha \gtrsim 1$), and was used to fit $\langle z \rangle$ in the main plot (solid blue line).

over a range of $\Delta\phi$. We find that quartic modes represent collective, primarily rotational motions of ellipses (cf. Fig. 2 inset), which do not lead to cage breaking and particle rearrangements. Thus, we expect that if the isostatic counting argument is reformulated so that quartic modes are not constrained, the average number of contacts $\langle z \rangle$ will correspond to the minimum number of contacts necessary to constrain the *quadratic* modes.

Isostaticity for frictionless ellipse packings assumes $\mathcal{N}\langle z \rangle_{\text{iso}}/2 = (2d - 1)\mathcal{N} - d + 1$, which includes a degree of freedom for particle compression. If it is unnecessary to constrain the quartic modes, this equation can be rewritten:

$$\frac{\mathcal{N}\langle z \rangle}{2} = (2d - 1)\mathcal{N} - d + 1 - N_1, \quad (2)$$

where $N_1 = i^*(\alpha) - d + 1$ is the number of quartic modes in region 1 of the frequency spectrum. By measuring N_1 , we can predict $\langle z \rangle(\alpha)$, which, as shown in Fig. 3, agrees with $\langle z \rangle$ measured in simulations. In the inset to Fig. 3, we show that $\mathcal{N}/N_1 - 1$ has two power-law regimes: $\sim\sqrt{\alpha - 1}$ for $\alpha - 1 \ll 1$ and $\sim(\alpha - 1)$ for $\alpha \gtrsim 1$. In these limits [7],

$$\langle z \rangle(\alpha) = \langle z \rangle(1) + A\sqrt{\alpha - 1} \quad \text{for } \alpha - 1 \ll 1 \quad (3)$$

$$= \langle z \rangle_{\text{iso}} - 1/(1 + B(\alpha - 1)) \quad \text{for } \alpha \gtrsim 1, \quad (4)$$

where $A, B > 0$. Equation (4) implies $\langle z \rangle = \langle z \rangle_{\text{iso}}$ as $\alpha \rightarrow \infty$, yet this remains an open question. We have demonstrated that hypostaticity in ellipse packings originates from quartic modes and that they are isostatic with respect to only *quadratic* modes.

Hypostaticity of shape-annealed packings.—The ellipse packings discussed to this point were generated using the compression method at fixed α . Since ellipse packings are hypostatic, it is possible to obtain packings with higher $\langle z \rangle$ than found previously without increasing order. To investigate this possibility, we developed a shape-annealing method that creates ellipse packings by incrementally increasing $\alpha > 1$. We initially generate bidisperse disk packings. Each particle is then assigned the same aspect ratio $1 + \Delta\alpha$ with the direction of the long axis chosen randomly. A new ellipse packing is formed from this initial state using the compression method. The particles of the new packing are elongated again along their major axes, and the protocol is repeated until a packing with the desired α is reached. Shape-annealing generates packings with $\langle z \rangle$ much closer to z_{iso} (Fig. 3). The annealed packings still exhibit quartic modes and N_1 can be used to predict $\langle z \rangle$ through (2). The predicted $\langle z \rangle$ shows excellent agreement with simulations even though the variation of N_1 with α differs significantly from that for “compressed” packings.

Mechanical properties.—To investigate the effect of quartic modes on mechanical properties of ellipse packings, we calculated the static bulk and shear moduli as a function of $\phi - \phi_J$ by measuring the response of the pressure tensor $p_{\alpha\beta}$ [18], with $\alpha, \beta = x, y$, to small compression and shear strains followed by energy minimization. To obtain the bulk and shear moduli, we measured $B = \phi dp/d\phi$ and $G = d\Sigma/d\gamma$, respectively, where pressure $p = d^{-1}\sum_{\alpha} p_{\alpha\alpha}$, shear stress $\Sigma = -p_{xy}$, and γ is the shear strain. p, Σ, B , and G are measured in units of ε/\sqrt{ab} , where ε is the spring energy. In the inset to Fig. 4(a), we show that B is roughly independent of $\phi - \phi_J$ for all α , which is identical to the near-affine scaling of B found for packings of spherical particles [2]. In contrast, in the main panel of Fig. 4(a), the shear modulus displays novel power-law scaling $G = G_0(\alpha)(\phi - \phi_J)^\tau$ with $\tau = 1$ compared to $\tau = 0.5$ for packings of spherical particles, and $G_0(\alpha) \sim (\alpha - 1)^{-0.5}$. The scaling exponent crosses over from 1 to 0.5 for $\Delta\phi \gtrsim \alpha - 1$.

To link the new scaling behavior of G with $\phi - \phi_J$ to the existence of quartic modes, we calculated the overlap of the displacement vector $\Delta\vec{\xi} = \vec{\xi} - \vec{\xi}_0$ (defined by subtracting the configuration variables of the strained packing $\vec{\xi}$ from those of the “unperturbed” packing $\vec{\xi}_0$) with each eigenvector of the dynamical matrix evaluated at $\vec{\xi}_0$. In Fig. 4(b), we plot $C(\omega_i) = \Delta\vec{\xi}/\Delta\xi \cdot \hat{e}_i$ versus ω_i for all shear strains (squares) and compressions (circles) used to calculate G and B at $\alpha = 1.05$ and $\Delta\phi = 10^{-3}$ for $N = 480$. The solid (dashed) lines represent the average over shear (compression) strains. The three discrete frequency regimes in Fig. 4(b) correspond to branches 1, 2, and 3 in Fig. 1. We find that compression does not excite quartic modes in branch 1 and only weakly excites modes in the quadratic rotational branch 2. In contrast, shear excites large contributions from the quartic modes, which are comparable to contributions from branches 2 and 3.

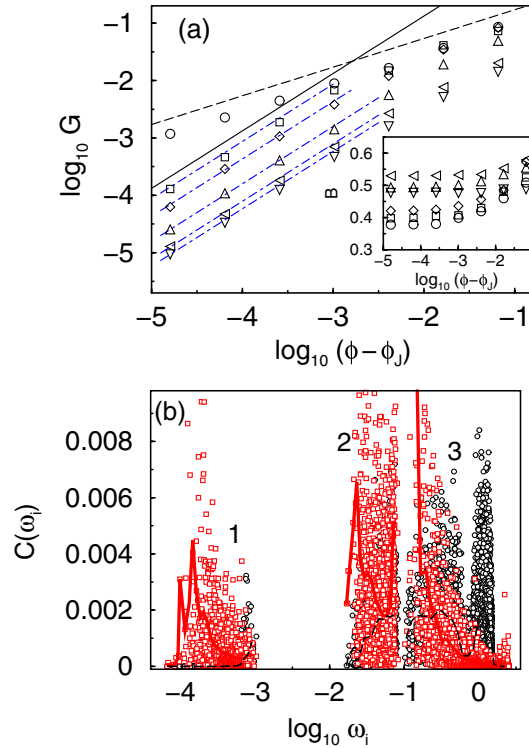


FIG. 4 (color online). (a) Static shear modulus G vs $\phi - \phi_J$ for ellipse packings with $N = 480$ at $\alpha = 1$ (circles), 1.002 (squares), 1.01 (diamonds), 1.1 (upward triangles), 1.5 (leftward triangles), and 2.0 (downward triangles). The solid (dashed) line has slope 1 (0.5). Dot-dashed lines show $G = 0.6(\phi - \phi_J)/(\alpha - 1)^{0.5}$. Inset: Bulk modulus B vs $\phi - \phi_J$. (b) Overlap $C(\omega_i)$ of displacements $\Delta \vec{\xi}$ following shear (squares) and compression (circles) with eigenvectors \hat{e}_i of the dynamical matrix at ξ_0 vs ω_i for strains used to calculate G and B at $\alpha = 1.05$ and $\Delta\phi = 10^{-3}$ for the system in (a). The solid (dashed) lines represent an average over shear (compression) strains.

Thus, the existence of quartic modes changes the mechanical properties of ellipse packings. We can explain the dependence of G on $\phi - \phi_J$ using the following scaling arguments. The shear modulus is related to the change in potential energy from shear strain:

$$G \approx \gamma^{-1} \Delta V(\gamma) = \sum_i \langle \Delta \vec{\xi} \cdot \hat{e}_i \rangle \omega_i^2 = \sum_{\nu=1}^3 N_\nu c_\nu \langle \omega^2 \rangle_\nu, \quad (5)$$

where the first sum is over vibrational modes i , N_ν is the number of modes in branch ν , and we have assumed $c_i = \langle \Delta \vec{\xi} \cdot \hat{e}_i \rangle$ is nearly constant *within* each branch. We find that the mean-square frequency of the quartic modes, $\langle \omega^2 \rangle_1$ scales as $\phi - \phi_J$, whereas the mean-square frequencies of the branches 2 and 3 are independent of ϕ in this regime. In addition, c_ν and N_ν depend strongly on α , but not $\phi - \phi_J$. The scaling $G \propto (\phi - \phi_J)$ can, therefore, be ascribed to the frequency dependence of the quartic modes, and thus the shear response of ellipse packings is significantly different from that for packings of spherical particles [2].

In conclusion, we find that particle asphericity qualitatively changes the jamming transition. Packings with spherical grains are exceptional: they are isostatic, and all nontrivial vibrational modes increase quadratically with deformation amplitude. In contrast, ellipse packings possess quartic modes characterized by collective rotational motions. These modes control the scaling of the shear modulus with $\phi - \phi_J$, and thus strongly affect the rigidity of ellipse packings. These results point to a new critical point at $\alpha > 1$ that controls the structure and dynamics of aspherical particles.

Support from NSF Grant No. DMR-0549762 (B. C. and M. M.), No. DMR-0448838 (C. S. O.) and No. DMS-0835742 (C. S.) is acknowledged. We thank D. Bi, A. Liu, S. Nagel, T. Witten, N. Xu, and Z. Zeravcic for comments.

Note added in proof.—During the workshop “Dynamical Heterogeneities in Glasses, Colloids, and Granular Media” in Leiden, we learned of similar work on vibrational modes in ellipsoid packings [19].

-
- [1] A. J. Liu and S. R. Nagel, *Nature (London)* **396**, 21 (1998).
 - [2] C. S. O’Hern, L. E. Silbert, A. J. Liu, and S. R. Nagel, *Phys. Rev. E* **68**, 011306 (2003).
 - [3] C. F. Moukarzel, *Phys. Rev. Lett.* **81**, 1634 (1998); R. Blumenfeld, *Phys. Rev. Lett.* **93**, 108301 (2004).
 - [4] H. A. Makse, D. L. Johnson, and L. M. Schwartz, *Phys. Rev. Lett.* **84**, 4160 (2000).
 - [5] C. S. O’Hern, S. A. Langer, A. J. Liu, and S. R. Nagel, *Phys. Rev. Lett.* **88**, 075507 (2002).
 - [6] M. Wyart, S. R. Nagel, and T. A. Witten, *Europhys. Lett.* **72**, 486 (2005).
 - [7] A. Donev, R. Connelly, F. H. Stillinger, and S. Torquato, *Phys. Rev. E* **75**, 051304 (2007).
 - [8] A. Donev, I. Cisse, D. Sachs, E. A. Variano, F. H. Stillinger, R. Connelly, and S. Torquato, *Science* **303**, 990 (2004).
 - [9] T. S. Majmudar and R. P. Behringer, *Nature (London)* **435**, 1079 (2005).
 - [10] S. Henkes, C. S. O’Hern, and B. Chakraborty, *Phys. Rev. Lett.* **99**, 038002 (2007).
 - [11] G.-J. Gao, J. Blawdziewicz, and C. S. O’Hern, *Phys. Rev. E* **74**, 061304 (2006).
 - [12] H. P. Zhang and H. A. Makse, *Phys. Rev. E* **72**, 011301 (2005).
 - [13] J. W. Perram and M. S. Wertheim, *J. Comput. Phys.* **58**, 409 (1985).
 - [14] J. W. Perram, J. Rasmussen, E. Praetgaard, and J. L. Lebowitz, *Phys. Rev. E* **54**, 6565 (1996).
 - [15] B. J. Berne and P. Pechukas, *J. Chem. Phys.* **56**, 4213 (1972).
 - [16] D. J. Cleaver, C. M. Care, M. P. Allen, and M. P. Neal, *Phys. Rev. E* **54**, 559 (1996).
 - [17] A. Tanguy, J. P. Wittmer, F. Leonforte, and J.-L. Barrat, *Phys. Rev. B* **66**, 174205 (2002).
 - [18] M. P. Allen and D. J. Tildesley, *Computer Simulation of Liquids* (Oxford University Press, New York, 1987).
 - [19] Z. Zeravcic, N. Xu, A. J. Liu, S. R. Nagel, and W. van Saarloos, <http://xxx.lanl.gov/abs/0904.1558>.